

Received 18 November 2023, accepted 27 November 2023, date of publication 5 December 2023, date of current version 13 December 2023.

Digital Object Identifier 10.1109/ACCESS.2023.3339762

RESEARCH ARTICLE

Analysis of the Influence of the Front Vehicle on the Propagation Loss of ETC System of the Back Vehicle

XIAOYU LI¹, WENBO ZENG², AND HUawei LIANG³

¹Faculty of Applied Science, The University of British Columbia, Vancouver, BC V6T 1Z4, Canada

²School of Electronic Information and Electrical Engineering, Changsha University, Changsha 410003, China

³Hefei Institutes of Physical Science, Chinese Academy of Science, Hefei 230031, China

Corresponding author: Xiaoyu Li (lixiaoyu800@gmail.com)

ABSTRACT As a typical application of intelligent transportation systems (ITS), the electronic toll collection (ETC) system has been widely used on highways due to its excellent toll efficiency. In the actual traffic environment, there usually exists more than one vehicle in the radiation area of the road-side units (RSU) at the same time, and the front vehicle will affect the ray paths between the RSU and the on-board units (OBU) of the back vehicle. Here we studied the front vehicle's impact on the ETC system's path propagation loss by ray tracing technology and Uniform Theory of Diffraction (UTD). Firstly, we simplified the vehicle body structure into two equivalent geometric models. Four situations were considered according to the vehicles' front and rear positions. We analyzed each scenario's propagation loss models under line-of-sight (LOS) and non-line-of-sight (NLOS) conditions based on the distance change among RSU, OBU, and the front vehicle. Finally, we developed an ETC comprehensive test equipment to measure the propagation loss of the four scenarios at a toll station. Both simulation and experiment results indicate that the propagation loss models proposed in this paper are valid.


INDEX TERMS Electronic toll collection, geometric features, propagation loss model, ray tracing, the front vehicle, uniform theory of diffraction.

I. INTRODUCTION

ELECTRONIC toll collection (ETC) system is an essential application of intelligent transportation system (ITS) and has been widely adopted in the highway, housing estates, and parking lots [1], [2], [3], [4], [5]. An ETC system consists of road-side units (RSU), on-board units (OBU) installed on the windshield of vehicles, and a cost accounting subsystem operating in the background [6], [7]. RSU connects to OBU (read or write information) through 5.8 GHz wireless communication technology called Dedicated Short Range Communication (DSRC) [8], [9], [10]. Researching highly accurate radio propagation prediction models is vital in designing and optimizing ETC systems, such as matching communication equipment, determining antenna height, and calculating communication distance [4], [11]. In actual appli-

cation scenarios, many moving and stationary objects like surrounding vehicles and infrastructure can reflect, scatter, diffract and even block the signals [12], [13], [14]. As a result, the received signal of the OBU/RSU is composed of many multipath signals with randomly distributed amplitudes and phases. Therefore, the research of ETC channel modeling considering multipath propagation characteristics is of great significance to the development of ITS.

The height of the transmitter (Tx) and receiver (Rx) antennas and their relative positions determine the multipath components in wireless communication [15], [16]. Compared with cellular systems [17], the antennas of the Tx and Rx in vehicular communication have relatively lower elevation angles, and other vehicles (surrounding vehicles) will become obstacles to the LOS signal between Tx and Rx [13], [18], resulting in distinct attenuation and packet loss [19], [20]. The influence of shadowing from other large vehicles (trucks or buses) on vehicular communication is analyzed in [13],

The associate editor coordinating the review of this manuscript and approving it for publication was Mohamed Kheir .

and it reveals that the bus will generate an additional 15-20 dB attenuation and an increase in the root-mean-square delay spread. In [21], In this paper, the 5-GHz obstructed V2V channels are characterized through measurement-calibrated ray-tracing simulations for different antenna deployments in the flat and sloped terrain environments. In existing studies [22], [23], ETC radio links are generally considered to operate under LOS conditions (see Figure 1(a)). However, most of the time, many vehicles line up to cross the ETC gate, as shown in Figure 1(b), from which we can see two or more vehicles simultaneously in the RSU antenna radiation area. The front vehicle will hinder the direct signal path between RSU and OBU on the back vehicle. In this case, the radio link propagating conditions should switch from LOS to NLOS conditions or LOS/NLOS mixed environments. Moreover, the NLOS condition causes multipath components and the loss of LOS components, leading to severe signal fading [19]. Thus, it is necessary and essential to explore the impact of front vehicles between RSU and OBU in the ETC link.

The ETC channel propagation loss models in the case of a single lane are established in [22], but it only regards the ground as the reflection surface. In [23], the differences in radio wave propagation caused by the head geometry characteristics of cab-over-engine and cab-behind-engine vehicles are analyzed, and it points out that the engine hood may cause reflection and diffraction of ray paths. However, it neglects the influence of the front vehicle. The attenuation of radio signals and the composition of multipath components are affected not only by the obstacle's position and material but also by the geometry features of the obstacle [24], [25], [26]. Therefore, in analyzing the ETC scene with the interference of the front vehicle, the geometric shape of the front vehicle and the back vehicle should be considered.

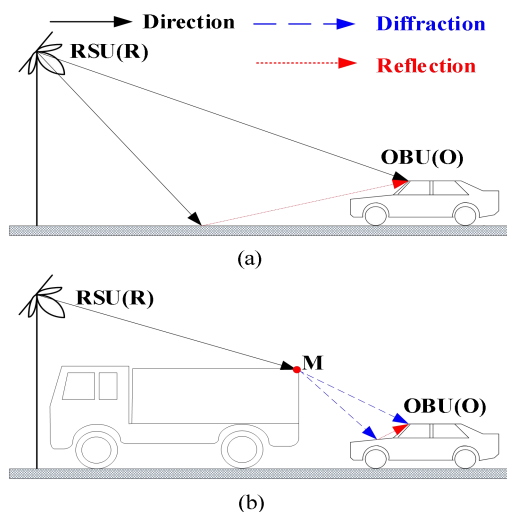


FIGURE 1. The application scenario of the ETC system. (a) One vehicle in the ETC lane. (b) More than one vehicle in the ETC lane.

In this paper, based on ray tracing technology [25], [27] and Uniform Theory of Diffraction (UTD) [28], [29], we analyze the impact of the front vehicle on the propagation loss between RSU and OBU. Specifically, the contributions of this work are presented as follows:

- Given the geometric commonality and the personality of different vehicle structures, we quantify the complex structure of the vehicles into two simplified models: cars (cab-over-engine vehicles) and trucks (cab-behind-engine vehicles). Four different ETC communication scenarios and corresponding propagation loss models are proposed based on the combination of cars and trucks and their relative positions.
- We discuss the interference of the front vehicle on the communication between the RSU and OBU according to the distance changes between the RSU, OBU, and the front vehicle. For each scene, we have calculated the existing conditions of each ray path and innovatively mapped them to the same coordinate axis plane, which is divided into different zones containing multiple types of ray paths.
- We have developed an ETC comprehensive test equipment based on a software-defined radio platform and successfully verified the effectiveness of the four propagation loss models we proposed at an ETC toll station.

The remainder of this paper is organized as follows: In section II, we briefly introduce four different propagation loss models, as illustrated in Figure. 2. Then, we analyze the propagation loss with the distance change among RSU, OBU, and the front vehicle. The simulation results are shown in section III. Details of the ETC comprehensive test instruments and the test vehicles are presented in section IV. Conclusions are proposed in the last section.

II. PROPAGATION LOSS MODELS

In this section, we concisely analyze the effects of the geometric features of the vehicle and the distance among OBU, the front vehicle, and RSU on the propagation mechanism zone. We divide the ETC application into four different propagation scenarios and propose their corresponding propagation loss models.

A. CHANNEL MODEL FOR V2R COMMUNICATION

This paper models the channel of an ETC communication system based on consistent diffraction theory, ray tracing technology, and geometric features of vehicles (cars and trucks). The model mainly considers the impact of front car interference on the ETC communication system. Discussed the impact of the distance between RSU and OBU, as well as the distance between the OBU and the front vehicle, on the propagation loss.

Ray tracing technology is a geometric ray technique based on theories such as reflection and refraction laws, which can accurately describe the multipath propagation of electromagnetic waves in wireless communication, such as direct,

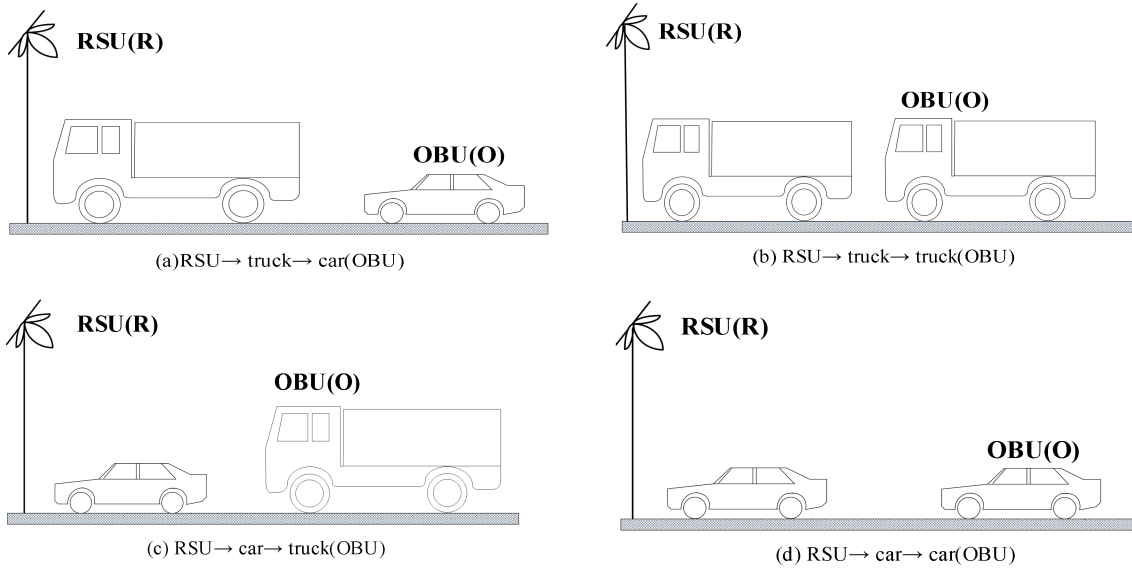


FIGURE 2. Four different propagation scenarios.

reflection, and scattering. The basic idea is to treat the transmitting end as the emission source, and each radio wave emitted by it is treated as a ray. The ray passes through various propagation paths such as direct radiation, reflection, and scattering to track the ray until it reaches the receiving end or the energy of the radio wave is lower than the considered limit. The received ray is vectorized and overlaid with field strength to obtain the signal strength of the receiving point and the influence of the radiation source.

Thus completing the prediction of channel propagation. The consistent diffraction theory is the development and extension of geometric diffraction theory based on geometric optics and geometric acoustics. The consistent diffraction theory solves the problem that geometric diffraction theory cannot have non-uniformity at the intersection of shaded and illuminated regions, and can calculate the field strength of diffraction at the edge of the transition region. The consistent diffraction theory can analyze the propagation characteristics of wireless channels in complex environments, and is currently widely used in research on intelligent transportation, airborne antennas, and large parking lot tolls.

The combination of ray tracing technology and consistent diffraction theory has jointly constructed a highly accurate modeling method for wireless communication systems. Through ray tracing technology, the ray path of electromagnetic waves in wireless communication is predicted, and then the received power of the receiving point is calculated using consistent diffraction theory to obtain the propagation loss of ETC communication systems.

B. PROPAGATION LOSS IN ETC SYSTEM

The ground, vehicles, buildings, and road infrastructure can cause reflection, scattering, and diffraction of radio signals in a vehicular communication system, known as the

multipath effect. Then the ray paths include incident, reflected, diffracted, and scattered paths. The toll level crossings in China are usually in open areas, and the adjacent toll lanes are widely separated. Due to the relatively low height of vehicle antennas, the front vehicles often have a more significant impact on propagation than surrounding buildings and static obstacles [19], [23], [31]. Consequently, this paper ignores the scattering ray path caused by adjacent vehicles, buildings, and road infrastructure. In addition, the car following the target vehicle will not affect the radio link between the RSU and OBU on the target vehicle. Hence the ETC plaza can be simplified as a single lane in open areas. The electromagnetic wave propagation between the RSU and OBU contains three primary ray paths: direct path (RSU to OBU), reflected path (caused by the ground, the front vehicle, or the object vehicle), and diffracted path (caused by the front vehicle or the object vehicle). Since the vehicles must pass through the ETC plaza at a low speed (less than 20 km/h), the Doppler frequency deviation caused by motion is ignored in this paper [23].

Let $H(A, f, d_i)$ be the transfer function from the RSU to the OBU. The received signal of the OBU includes direct path, reflected path, and diffracted path component, then $H(A, f, d_i)$ can be expressed as:

$$H(A, f, d_i) = H_{\text{dir}}(A_{\text{dir}}, f, d_d) + H_{\text{ref}}(A_{\text{ref}}, f, d_r) + H_{\text{dif}}(A_{\text{dif}}, f, d_{\text{dr}}) \quad (1)$$

where A is the amplitude fading factor, f is the frequency, d_i is the transmission distance of different ray paths, d_d , d_r , and d_{dr} are the transmission distance of the direct path, reflected path, and diffracted path, respectively. $H_{\text{dir}}(A_{\text{dir}}, f, d_d)$, $H_{\text{ref}}(A_{\text{ref}}, f, d_r)$, and $H_{\text{dif}}(A_{\text{dif}}, f, d_{\text{dr}})$ are the transfer function of the direct path, reflected path, and diffracted path, respectively.

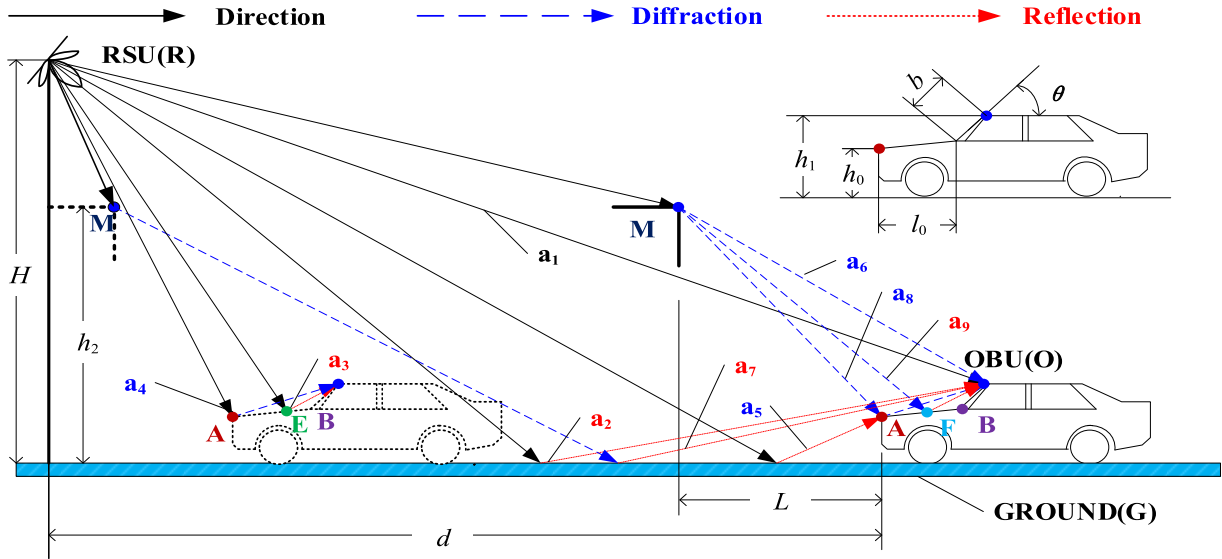


FIGURE 3. Nine ray paths in RSU→truck→car (OBU) scenario, a_1 is direct path R→O, a_2 is ground-reflected path R→G→O, a_3 is engine hood-reflected path R→E→O, a_4 is engine hood-diffracted path R→A→O, a_5 is ground-reflected/engine hood-diffracted path R→G→A→O, a_6 is front vehicle-diffracted path R→M→O, a_7 is front vehicle-diffracted/ground-reflected path R→M→G→O, a_8 is front vehicle-diffracted/engine hood-diffracted path R→M→A→O, a_9 is front vehicle-diffracted/engine hood-reflected path R→M→F→O.

Finally, the propagation loss between the RSU and OBU can be defined as [22]:

$$\begin{aligned}
 PL &= -20 \log_{10} |H(A, f, d_i)| \\
 &= -20 \log_{10} \left| \begin{matrix} H_{\text{dir}}(A_{\text{dir}}, f, d_d) + H_{\text{ref}}(A_{\text{ref}}, f, d_r) \\ + H_{\text{dif}}(A_{\text{dif}}, f, d_{\text{dr}}) \end{matrix} \right| \quad (2)
 \end{aligned}$$

C. FOUR DIFFERENT PROPAGATION SCENARIOS

According to the geometric characteristics of vehicles, the vehicle can be sorted into two classes, cab-over-engine vehicles (bus and truck) and cab-behind-engine vehicles (car) [22]. Based on the categories of vehicles, four different propagation scenarios are divided and discussed in this paper, as depicted in Figure 2. Meanwhile, the relative position among RSU, OBU, and the obstruction (the front vehicles) decides the types and areas of ray paths. When a signal is reflected and diffracted more than twice, the effect of reflection and diffraction on propagation loss is weak, so we only consider the primary and secondary reflection and diffraction in this paper.

1) RSU→TRUCK→CAR(WITH OBU INSTALLED)

As illustrated in Figure 2(a), the ray path can be affected by the truck’s rear cover and the car’s engine hood. According to whether the rear cover of the truck obstructs the direct path (a_1), the situation can be divided into LOS and NLOS. Figure 3 shows there always exist diffracted paths, R→M→O (a_6) and R→M→A→O (a_8). For cab-behind-engine vehicles, the bulgy engine hood and relative positions among OBU, bulgy engine hood, and RSU directly determine the reflected ray path (reflected from the ground or the engine hood) and diffracted ray path. Based on the geometric analysis of the reflection and diffraction path, this propagation model has nine ray paths (see Figure 3).

When the distance between the RSU and the OBU and between the front vehicle and the OBU changes, the effect of the rear cover of the truck and engine hood also changes. Therefore, in some areas, some ray paths may be blocked.

Suppose H and h_2 are the vertical height of RSU and truck from the ground, respectively, h_1 and h_0 are the vertical height of the top of the car and its engine hood from the ground, respectively, l_0 is the length of the engine hood, θ is the tilt angle of the front windshield of the car, b is the length of the front windshield of the car, d is the horizontal distance between RSU and the back vehicle, L is the horizontal distance between the front vehicle and the back vehicle ($d \geq L$), d_1 , d_2 and d_3 are the extreme distance of ground-reflected path, engine hood (front vertex)-reflected path and the engine hood (rear vertex)-reflected path, respectively (the detailed deduction can be seen in [23]).

Using the principle of similar triangles, we calculate the critical horizontal distance between the front and back vehicles where each ray path exists or vanishes.

- 1) The critical distance L_{a0} where the direct path (a_1) is blocked:

$$L_{a0} = \frac{(h_2 - h_1)(d + l_0 + b \cos \theta)}{H - h_1} - (l_0 + b \cos \theta) \quad (3)$$

- 2) The critical distance L_{a1} where the ground-reflected path (a_2) is blocked:

$$\begin{aligned}
 L_{a1} &= \begin{cases} d, & 0 \leq d < d_1 \\ \frac{(h_1 + h_2)d - (H - h_2)(l_0 + b \cos \theta)}{H + h_1}, & d \geq d_1 \end{cases} \quad (4)
 \end{aligned}$$

- 3) The critical distance L_{a2} where the engine hood-reflected path (a₃) is blocked:

$$L_{a2} = \begin{cases} \frac{(h_1+h_2-2h_0)d-(H-h_2)(l_0+b \cos \theta)}{H+h_1-2h_0}, & d_3 \leq d \leq d_2 \\ d, & \text{else} \end{cases} \quad (5)$$

- 4) The critical distance L_{a3} where the engine hood-diffracted path (a₄) is blocked:

$$L_{a3} = \frac{h_2 - h_0}{H - h_0} d \quad (6)$$

- 5) The critical distance L_{a4} where the ground-reflected/engine hood-diffracted path (a₅) is blocked:

$$L_{a4} = \frac{h_2 + h_0}{H + h_0} d \quad (7)$$

- 6) The critical distance L_{a5} where the front vehicle-diffracted/ ground-reflected path (a₇) is blocked:

$$L_{a5} = \frac{(h_2 + h_0)(l_0 + b \cos \theta)}{h_1 - h_0} \quad (8)$$

- 7) The critical distance L_{a6} where the front vehicle-diffracted/engine hood-diffracted path (a₈) exists:

$$L_{a6} = \frac{h_2 - h_0}{h_1 - h_0} (l_0 + b \cos \theta) \quad (9)$$

- 8) The critical distance L_{a7} where the front vehicle-diffracted/engine hood-diffracted path (a₈) is blocked:

$$L_{a7} = \frac{h_2 - h_0}{h_1 - h_0} (b \cos \theta) - l_0 \quad (10)$$

- 9) The critical distance L_{a8} where the ray paths (a₆, a₇, a₈, a₉) related to the front truck exist:

$$L_{a8} = d \quad (11)$$

Put all the critical distance data into a coordinate plane, which is divided into 24 zones (see Figure 4). The types of ray paths included in each region are presented in Table 1. For example, zone 22 in the figure, can be derived. L_{a0} is the critical distance for blocking the direct path. The direct path only exists when the distance between the two workshops is greater than L_{a0} , so zone 22 contains the direct path a₁. Similarly, zone 22 is located above L_{a3} , L_{a5} , L_{a6} , and L_{a7} . At this point, the distance between the two workshops is greater than the critical distance, so there are paths a₄, a₆, a₇, and a₈.

TABLE 1. The ray paths contained in each zone in RSU→truck→car.

Zone	Ray paths
1,15	(a ₁), (a ₄), (a ₅), (a ₆), (a ₈)
2,16	(a ₁), (a ₄), (a ₆), (a ₈)
3,17	(a ₁), (a ₆), (a ₈)
4,18	(a ₆), (a ₈)
5	(a ₁), (a ₄), (a ₅), (a ₆), (a ₈), (a ₉)
6	(a ₁), (a ₄), (a ₆), (a ₈), (a ₉)
7,11	(a ₁), (a ₆), (a ₈), (a ₉)
12	(a ₆), (a ₈), (a ₉)
8	(a ₁), (a ₃), (a ₄), (a ₅), (a ₆), (a ₈), (a ₉)
9	(a ₁), (a ₃), (a ₄), (a ₆), (a ₈), (a ₉)
10	(a ₁), (a ₃), (a ₆), (a ₈), (a ₉)
13	(a ₁), (a ₃), (a ₄), (a ₅), (a ₆), (a ₈)
14	(a ₁), (a ₃), (a ₄), (a ₆), (a ₈)
19	(a ₁), (a ₂), (a ₄), (a ₅), (a ₆), (a ₇), (a ₈)
20	(a ₁), (a ₄), (a ₅), (a ₆), (a ₇), (a ₈)
21	(a ₁), (a ₄), (a ₅), (a ₆), (a ₇), (a ₈)
22	(a ₁), (a ₄), (a ₆), (a ₇), (a ₈)
23	(a ₁), (a ₆), (a ₇), (a ₈)
24	(a ₆), (a ₇), (a ₈)

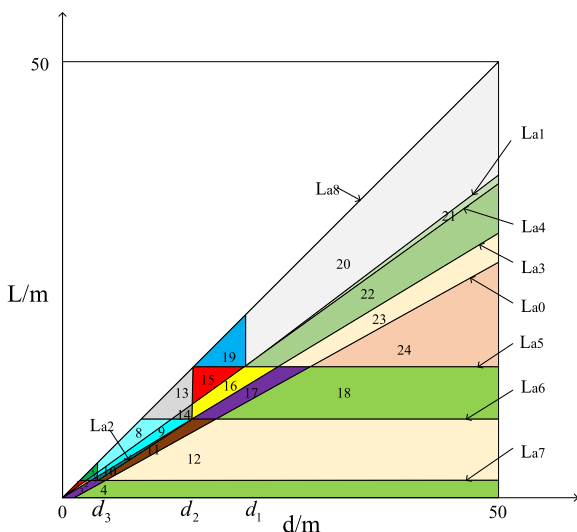


FIGURE 4. The axis formed by all the critical distance of the ray paths in RSU→truck→car (the same color represents the same path).

2) RSU→TRUCK→TRUCK(WITH OBU INSTALLED)

Figure 2(b) depicts that the ray path can be influenced by the rear cover of the front truck. As shown in Figure 5, because the height of the rear cover is not higher than that of the headstock of the truck, there is always a direct path R→O (b₁). In other words, the LOS condition exists for all time. Meanwhile, the ray path from RSU diffracts through the front truck's rear vertex (point M).

As a result, the propagation loss model has four kinds of ray paths.

Assume that h_2' is the vertical height of the truck's rear cover from the ground. The critical horizontal distances between the front vehicle and the back vehicle where each ray path exists or vanishes are as follows:

- 1) The critical distance L_{b1} where the ground-reflected path (b₂) is blocked:

$$L_{b1} = \frac{h_2' + h_2}{H + h_2'} d \quad (12)$$

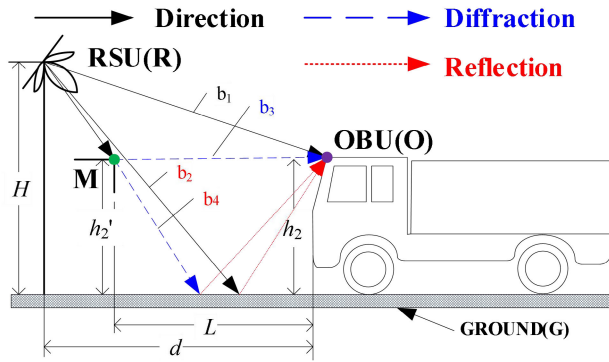


FIGURE 5. Four ray paths in RSU→truck→truck (OBU) scenario, b_1 is direct path R→O, b_2 is ground-reflected path R→G→O, b_3 is front vehicle-diffracted path R→M→O, b_4 is front vehicle-diffracted/ground-reflected path R→M→G→O.

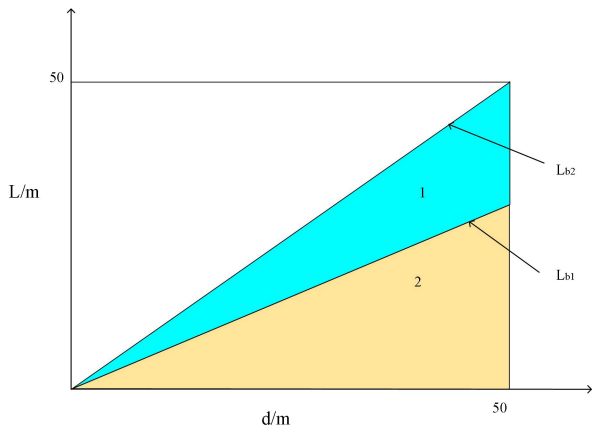


FIGURE 6. The axis formed by all the critical distances of the ray paths in RSU→truck→truck.

- 2) The critical distance L_{b2} where the ray paths (b_3, b_4) related to the front truck exists:

$$L_{b2} = d \tag{13}$$

The zoom maps and the types of ray paths each area contains are shown in Figure 6 and Table 2. For example, the zone 1 is located on the left side of the blocking ground reflection path L_{b1} , so ground emission path b_2 exists, so paths $b_1, b_3,$ and b_4 also exist.

TABLE 2. The ray paths contained in each zone in RSU→truck→truck.

Zone	Ray paths
1	(b_1), (b_2), (b_3), (b_4)
2	(b_1), (b_3), (b_4)

3) RSU→CAR→TRUCK(WITH OBU INSTALLED)

As presented in Figure 2(c), the ray path can be affected by the front car's rear cover and windshield. When electromagnetic waves pass through the windshield, most penetrate, and only

a few are reflected. Therefore, this paper ignores the reflected ray path caused by the rear windshield. According to Figure 7, there are nine ray paths in this propagation loss model, where the rear cover of the car has two points, C and D, to generate diffraction.

Suppose h_1' and h_0' are the vertical height of the car and its rear cover from the ground, respectively, l_0' is the length of the car's rear cover, l_1' is the length of the car.

The critical horizontal distances between the front vehicle and the back vehicle where each ray path exists or vanishes are as follows:

- 1) The critical distance L_{c0} where the diffracted paths (c_5, c_8) caused by point D is blocked:

$$L_{c0} = d - \frac{(H - h_0')l_0'}{h_1' - h_0'} \tag{14}$$

- 2) The critical distance L_{c1} where the ground-reflected path (c_2) is blocked by point D:

$$L_{c1} = \frac{h_0' + h_2}{H + h_2} d \tag{15}$$

- 3) The critical distance L_{c2} where the ground-reflected path (c_2) is blocked by point C:

$$L_{c2} = \frac{h_1' + h_2}{H + h_2} d - l_0' \tag{16}$$

- 4) The critical distance L_{c3} where the vehicle surface-reflected path (c_3) exists:

$$L_{c3} = \frac{h_2 - h_1'}{H + h_2 - 2h_1'} d - l_0' \tag{17}$$

- 5) The critical distance L_{c4} where the vehicle surface-reflected path (c_3) is blocked:

$$L_{c4} = \frac{h_2 - h_1'}{H + h_2 - 2h_1'} d - l_0' - l_1' \tag{18}$$

- 6) The critical distance L_{c5} where the front vehicle-diffracted/ground-reflected path (c_7) is blocked:

$$L_{c5} = \frac{h_0' + h_2}{h_1' - h_0'} l_0' \tag{19}$$

- 7) The critical distance L_{c6} where the front vehicle-diffracted/the rear cover reflected path (c_9) exists:

$$L_{c6} = \frac{h_2 - h_0'}{h_1' - h_0'} l_0' \tag{20}$$

- 8) The critical distance L_{c7} where the ray paths ($c_3, c_4, c_5, c_6, c_7, c_8, c_9$) related to the front vehicle exist:

$$L_{c7} = d \tag{21}$$

The zoom maps and the types of ray paths that each area includes are presented in Figure 8 and Table 3. For example, for the zone 16, as the vehicle ahead is a sedan, the direct path c_1 always exists, and similarly, paths c_4 and c_6 also exist. Due to the location of zone 16 above $L_{c1}, L_{c2},$ and L_{c7} , paths c_2 and c_7 exist.

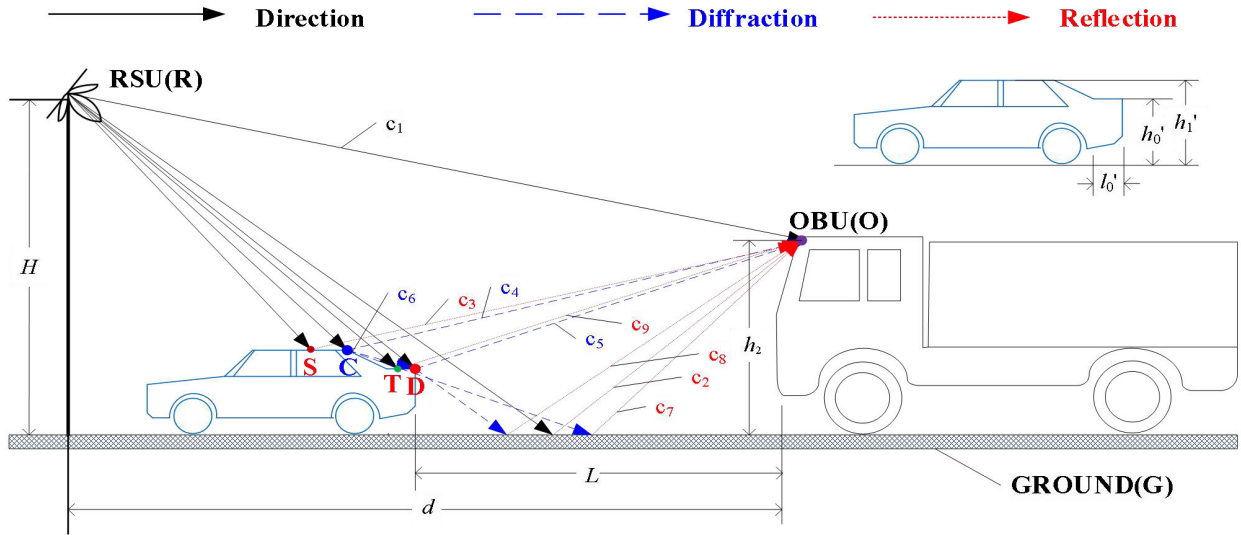


FIGURE 7. Nine ray paths in RSU→car→truck (OBU) scenario, c_1 is direct path R→O, c_2 is ground-reflected path R→G→O, c_3 is vehicle surface-reflected path R→S→O, c_4 is the rear cover diffracted path R→C→O, c_5 is the rear cover diffracted path R→D→O, c_6 is the rear cover diffracted path R→C→D→O, c_7 is front vehicle-diffracted/ground-reflected path R→C→G→O, c_8 is front vehicle-diffracted/ground-reflected path R→D→G→O, c_9 is front vehicle-diffracted/the rear cover-reflected path R→C→T→O.

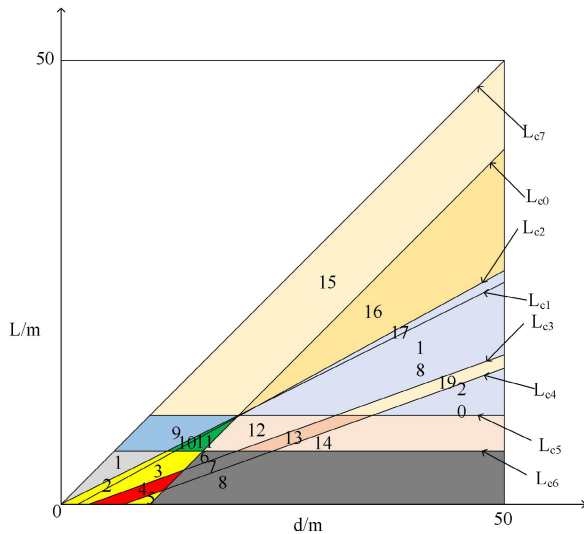


FIGURE 8. The axis formed by all the critical distances of the ray paths in RSU→car→truck.

4) RSU→CAR→CAR(WITH OBU INSTALLED)

As shown in Figure 2(d), the rear cover of the front car and the engine hood of the rear car will affect the ray path. We can see from Figure 10 that there are 12 ray paths in the propagation loss model.

The critical horizontal distances between the front vehicle and the back vehicle where each ray path exists or vanishes are as follows:

- 1) The critical distance L_{d0} where the diffracted path (d_{10} , d_{11} , d_{12}) caused by point D is blocked:

$$L_{d0} = d - \frac{(H - h_0')l_0'}{h_1' - h_0'} \quad (22)$$

TABLE 3. The ray path contained in each zone in RSU→car→truck.

Zone	Ray Paths
1	(c_1), (c_2), (c_4), (c_5), (c_6), (c_8), (c_9)
2,3,5	(c_1), (c_4), (c_5), (c_6), (c_8), (c_9)
4	(c_1), (c_3), (c_4), (c_5), (c_6), (c_8), (c_9)
6,8	(c_1), (c_4), (c_6), (c_9)
7	(c_1), (c_3), (c_4), (c_6), (c_9)
9	(c_1), (c_2), (c_4), (c_5), (c_6), (c_8)
10,11	(c_1), (c_4), (c_5), (c_6), (c_8)
12,14	(c_1), (c_4), (c_6)
13	(c_1), (c_3), (c_4), (c_6)
15	(c_1), (c_2), (c_4), (c_5), (c_6), (c_7), (c_8)
16	(c_1), (c_2), (c_4), (c_6), (c_7)
17,18,20	(c_1), (c_4), (c_6), (c_7)
19	(c_1), (c_3), (c_4), (c_6), (c_7)

- 2) The critical distance L_{d1} where the engine hood of the car blocks the ground-reflected path (d_2):

$$L_{d1} = \begin{cases} d, & 0 \leq d < d_1 \\ \frac{(h_1 + h_1')d - (H - h_1')(l_0 + b \cos \theta)}{H + h_1}, & d \geq d_1 \end{cases} \quad (23)$$

- 3) The critical distance L_{d2} where the engine hood-reflected path (d_3) is blocked:

$$L_{d2} = \begin{cases} 0, & d_3 \leq d \leq d_2 \\ d, & \text{else} \end{cases} \quad (24)$$

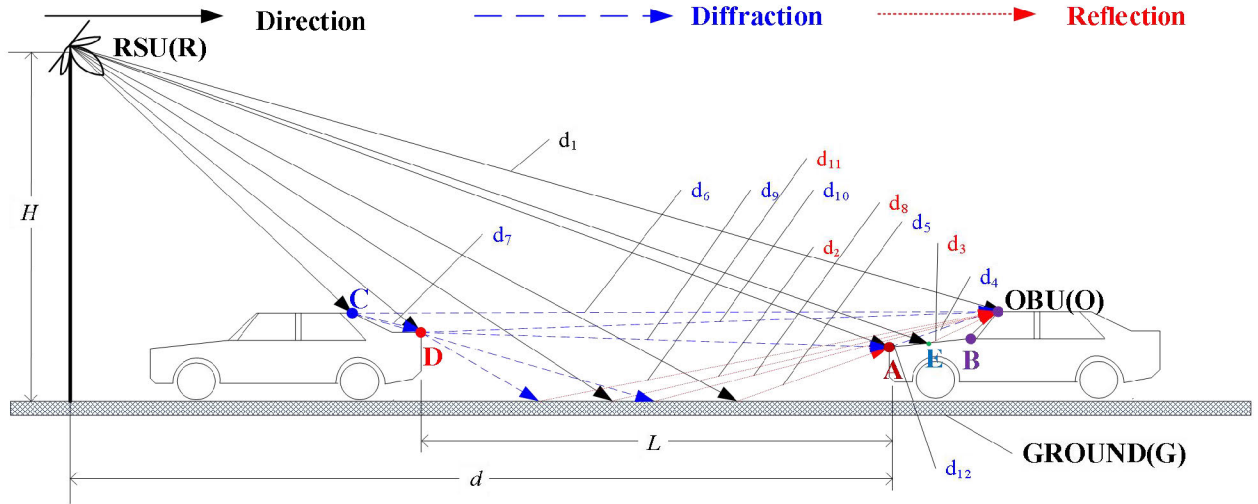


FIGURE 9. Twelve ray paths in RSU→car→car (OBU) scenario, d_1 is direct path R→O, d_2 is ground-reflected path R→G→O, d_3 is engine hood-reflected path R→E→O, d_4 is engine hood-diffracted path R→A→O, d_5 is ground-reflected/engine hood-diffracted path R→G→A→O, d_6 is the rear cover diffracted path R→C→O, d_7 is the rear cover diffracted path R→C→D→O, d_8 is the rear cover diffracted/ground-reflected path R→C→G→O, d_9 is the rear cover diffracted/the engine hood diffracted path R→C→A→O, d_{10} is the rear cover diffracted path R→D→O, d_{11} is the rear cover diffracted/ground-reflected path R→D→G→O, d_{12} is the rear cover diffracted/the engine hood diffracted path R→D→A→O.

- 4) The critical distance L_{d3} where the ground-reflected/engine hood-diffracted path (d_5) is blocked by point D:

$$L_{d3} = \frac{h_0' + h_0}{H + h_0} d \quad (25)$$

- 5) The critical distance L_{d4} where the ground-reflected path (d_2) is blocked by point C:

$$L_{d4} = \frac{h_1' + h_0}{H + h_0} d - l_0' \quad (26)$$

- 6) The critical distance L_{d5} where the rear cover diffracted/ground-reflected path caused by point C (d_8) is blocked:

$$L_{d5} = \frac{h_0' + h_1}{h_1' - h_0'} l_0' \quad (27)$$

- 7) The critical distance L_{d6} where the rear cover diffracted/ground-reflected path caused by point D (d_{11}) is blocked:

$$L_{d6} = \frac{(h_0' + h_0)(l_0 + b \cos \theta)}{h_1 - h_0} \quad (28)$$

- 8) The critical distance L_{d7} where the ray paths ($d_6, d_7, d_8, d_9, d_{10}, d_{11}, d_{12}$) related to the front vehicle exist:

$$L_{d7} = d \quad (29)$$

The zoom maps and the types of ray paths each area includes are presented in Figure 10 and Table 4. For example, in Figure 10, For the zone 11, as both the front and rear cars are sedans, the direct path d_1 always exists. zone 11 is located below L_{d2} , to the left of L_{d1} , so paths d_2 and d_3 do not exist. And because the zone 11 is located above L_{d3}, L_{d4}, L_{d5} , and L_{d6} , paths $d_4, d_5, d_6, d_7, d_8, d_9, d_{10}, d_{11}$, and d_{12} exist.

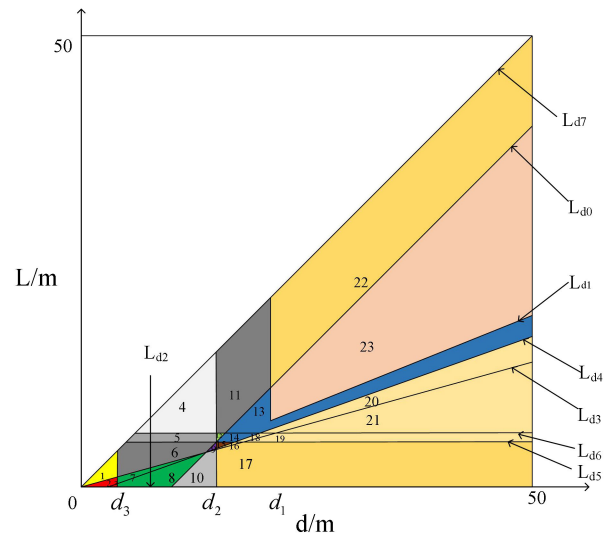


FIGURE 10. The axis formed by all the critical distance of the ray paths in RSU→car→car.

D. PROPAGATION LOSS MODELS

As depicted in sections II-A and B, the propagation loss of different scenarios can be expressed as:

$$PL = -20 \log_{10} \left| \sum_{i=0}^n H_i(A_i, f, d_i) \right| \quad (30)$$

where n is the number of ray paths.

The transfer functions of the direct path, reflected path and diffracted path are as follows:

$$H_{dir}(A_{dir}, f, d_d) = \frac{\lambda}{4\pi d_d} \exp(-jkd_d) \quad (31)$$

TABLE 4. The ray paths contained in each zone in RSU→car→car.

Zone	Ray paths
1,3	(d ₁), (d ₄), (d ₅), (d ₆), (d ₇), (d ₉), (d ₁₀), (d ₁₂)
2,3,5	(d ₁), (d ₄), (d ₆), (d ₇), (d ₉), (d ₁₀), (d ₁₂)
4	(d ₁), (d ₃), (d ₄), (d ₅), (d ₆), (d ₇), (d ₈), (d ₉), (d ₁₀), (d ₁₁), (d ₁₂)
5	(d ₁), (d ₃), (d ₄), (d ₅), (d ₆), (d ₇), (d ₈), (d ₉), (d ₁₀), (d ₁₂)
6	(d ₁), (d ₃), (d ₄), (d ₅), (d ₆), (d ₇), (d ₉), (d ₁₀), (d ₁₂)
7,8	(d ₁), (d ₃), (d ₄), (d ₆), (d ₇), (d ₉), (d ₁₀), (d ₁₂)
9	(d ₁), (d ₃), (d ₄), (d ₅), (d ₆), (d ₇), (d ₉)
10	(d ₁), (d ₃), (d ₄), (d ₆), (d ₇), (d ₉)
11	(d ₁), (d ₄), (d ₅), (d ₆), (d ₇), (d ₈), (d ₉), (d ₁₀), (d ₁₁), (d ₁₂)
12	(d ₁), (d ₄), (d ₅), (d ₆), (d ₇), (d ₈), (d ₉), (d ₁₀), (d ₁₂)
13,14	(d ₁), (d ₄), (d ₅), (d ₆), (d ₇), (d ₈), (d ₉)
15	(d ₁), (d ₄), (d ₅), (d ₆), (d ₇), (d ₉)
16,17	(d ₁), (d ₄), (d ₆), (d ₇), (d ₉)
18,19,20,21	(d ₁), (d ₄), (d ₆), (d ₇), (d ₈), (d ₉)
22	(d ₁), (d ₂), (d ₄), (d ₅), (d ₆), (d ₇), (d ₈), (d ₉), (d ₁₀), (d ₁₁), (d ₁₂)
23	(d ₁), (d ₂), (d ₄), (d ₅), (d ₆), (d ₇), (d ₈), (d ₉)

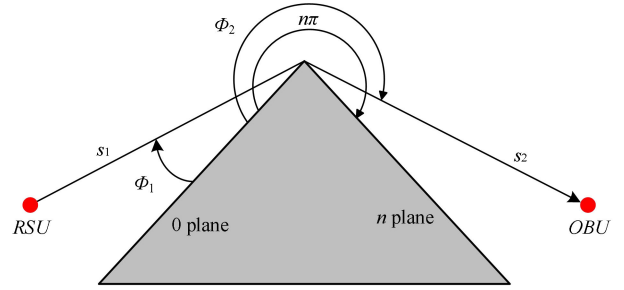


FIGURE 11. Consistent diffraction geometry.

R_{ri} is the reflection coefficient [15], [20], which can be calculated by:

$$R_{ri} = \frac{\cos \theta_i - \alpha_i t_i}{\cos \theta_i + \alpha_i t_i} \quad (38)$$

where θ_i is the incidence angle, when $\alpha_i = 1$, R_{ri} is the horizontal polarization reflection coefficient; when $\alpha_i = 1/\epsilon_i$, R_{ri} is the vertical polarization reflection coefficient. $\epsilon_i = \epsilon_2/\epsilon_1$ is the relative dielectric constant, ϵ_1 and ϵ_2 are the relative permittivity of the incident medium and the transmitted medium, $t_i = \sqrt{\epsilon_i - \sin^2 \theta_i}$.

III. SIMULATION RESULTS

In this part, we simulated the propagation loss of four models. The model parameters are presented in Table 5.

We assume that $H = 6$ m, $h_2 = h_2' = 4$ m, $h_1 = h_1' = 1.5$ m, $h_0 = h_0' = 1$ m, $l_0 = l_0' = 1$ m, $l_1' = 1.5$ m, $bsin\theta = 0.5$ m, $bcos\theta = 0.5$ m. With the change of L (the distance between the front vehicle and the back vehicle) and d (the distance between the RSU and the OBU), we can get different propagation path loss, as illustrated in Figure 12. The transmit power of RSU is 30dBm and the receive sensitivity of OBU is -30dBm. When the path loss is greater than 60dB, the OBU cannot be active. In order to distinguish the identification area more clearly, the area where the path loss is greater than 60db is indicated in black, we can get the bicolor heat map of propagation path loss, as illustrated in Figure 13. We can conclude from Figure 12 and Figure 13:

- 1) When L increases and d remains constant, the propagation loss changes from high to low and then to high; when L is constant, with the increase of d , the propagation loss also changes from high to low and then to high.
- 2) The propagation loss is relatively high when $d = L$ or $L = 0$. For instance, the propagation loss is between 55 dB and 70 dB when $d = L$ or $L = 0$ in Figure 13(a). We can regard the RSU and the front vehicle as a whole when $d = L$; the front vehicle and the back vehicle with OBU can be considered as a whole when $L = 0$. In the two situations, the front vehicle acts as an internal interference factor in the communication between the RSU and the OBU, resulting in a significant impact.

$$H_{ref}(A_{ref}, f, d_{ri}) = \frac{\lambda}{4\pi d_r} R_{ri} \exp(-jk d_{ri}) \quad (32)$$

$$H_{dif}(A_{dif}, f, d_{dr}) = \frac{\lambda}{4\pi s'} D \sqrt{\frac{s'}{s'(s'+s)}} \exp(-jk(s'+s)) \quad (33)$$

$$D = \frac{-\exp(-j\pi/4)}{2n\sqrt{2\pi k}} \left\{ \begin{array}{l} \cot\left(\frac{\pi+\beta_-}{2n}\right) F(kLa^+(\beta_-)) \\ + \cot\left(\frac{\pi-\beta_-}{2n}\right) F(kLa^-(\beta_-)) \\ + R_0 \cot\left(\frac{\pi-\beta_+}{2n}\right) F(kLa^-(\beta_+)) \\ + R_n \cot\left(\frac{\pi+\beta_+}{2n}\right) F(kLa^+(\beta_+)) \end{array} \right\} \quad (34)$$

$$F(x) = 2j\sqrt{x} \cdot \exp(jx) \cdot \int_{\sqrt{x}}^{\infty} \exp(-jt^2) dt \quad (35)$$

$$L = \frac{s_2 \cdot s_1}{s_2 + s_1} \quad (36)$$

$$a^\pm(\beta) = 2 \cos^2\left(\frac{2n\pi N^\pm - \beta}{2}\right) \quad (37)$$

where λ is the wavelength, k is the wavenumber, D is the diffraction coefficient (In [36], [37]), D mainly depends on the incident Angle, the Angle of diffraction, the edge material where diffraction occurs, and the reflection coefficient of the edge material. Φ_1 is the incidence Angle, Φ_2 is the diffraction Angle, $\beta_+ = \Phi_1 + \Phi_2$, $\beta_- = \Phi_1 - \Phi_2$, n is the wedge Angle (a multiple of π radians), R_0 and R_n are the reflection coefficients of the 0 and n planes, $F(x)$ is the Fresnel integral, and N^2 is the integer closest to satisfying the formula $N^2 = \beta \pm \pi/2n\pi$. The geometric diagram of the consistent diffraction is shown in Figure 11.

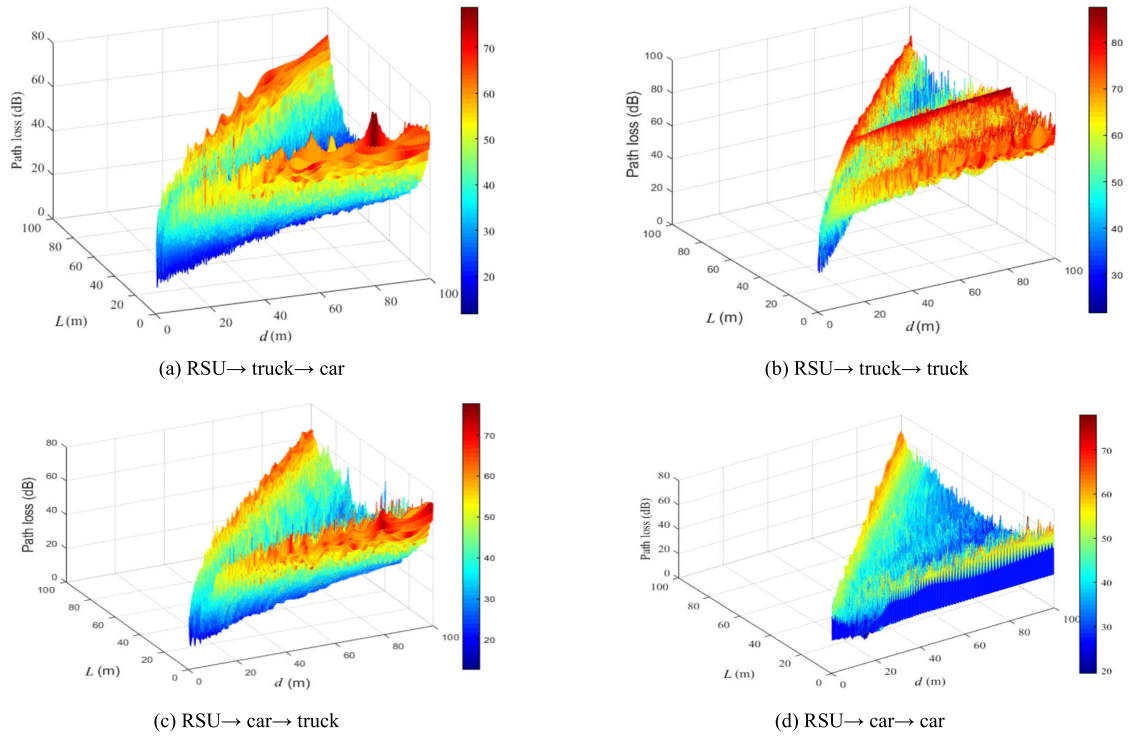


FIGURE 12. The propagation path loss of four propagation loss models.

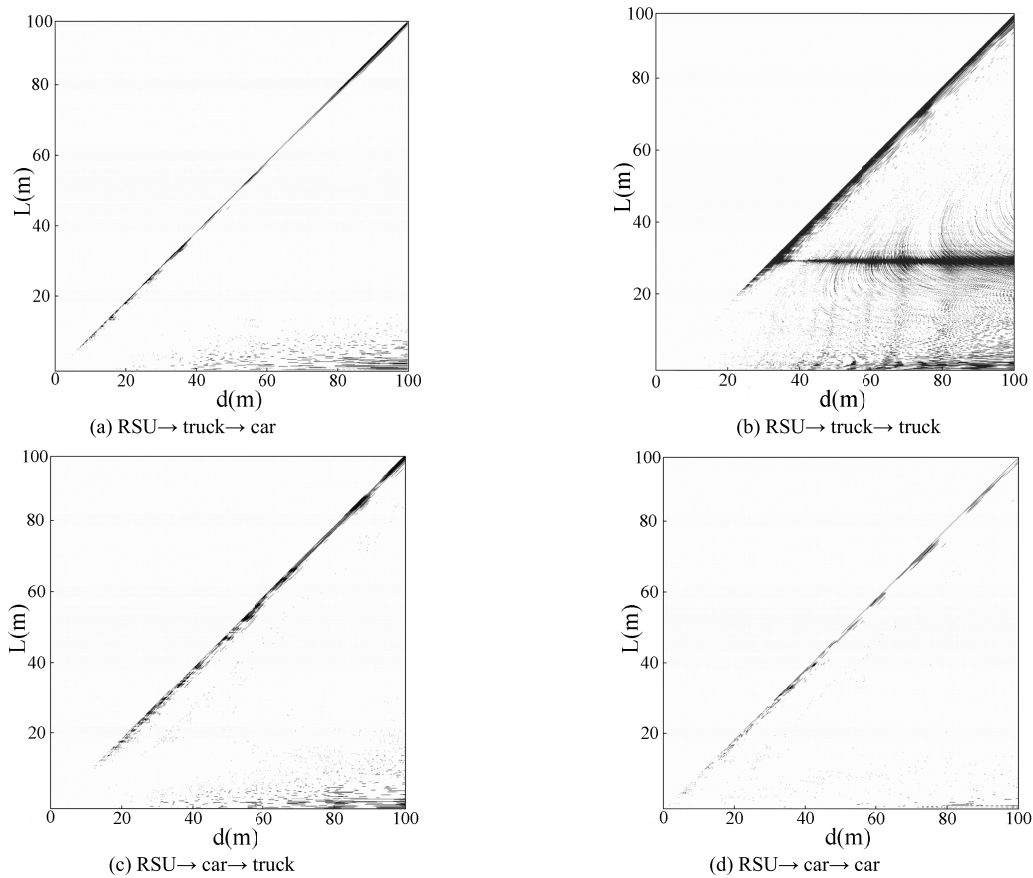
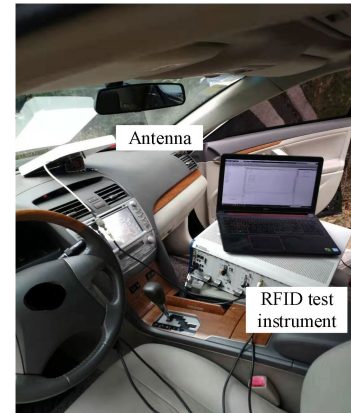


FIGURE 13. The bicolor heatmap of four propagation loss models.

- 3) Abrupt changes exist in all the propagation loss models because when the incidence angle approaches 0° or 180° (boundary points), the propagation loss is approximately zero, and a region near zero appears in the diffracted path. If there are one or more diffracted paths in the propagation loss model, such as Figure 13(a), (b), and (c), a relatively apparent low loss linear region appears. If there are more than two diffracted paths, such as Figure 13(d), a low loss triangular region occurs due to the cumulative effect of multiple diffracted incidence paths.
- 4) As shown in Figure 13(b), when L is about 30.6 m, there is a horizontal line with a sudden increase in the propagation loss. This model assumes that the two trucks are the same height. In the ray path $R \rightarrow M \rightarrow G \rightarrow O$, when $L = 30.6$ m, the reflection coefficient of the road surface is close to zero, so total reflection occurs, and the reflected wave cannot reach the OBU, leading to a rise in the path loss.

TABLE 5. Model parameters.

Parameters	Value
Road relative dielectric constant (ϵ_{r1})	15
Car hood relative dielectric constant (ϵ_{r2})	3.5
Air permeability (μ_{r1})	1
Air relative dielectric constant	1
Alloy film permeability (μ_{r2})	2
Alloy film relative dielectric constant	5
Glass permeability (μ_{r3})	1
Glass relative dielectric constant	4

**FIGURE 14. The test instruments.****FIGURE 15. Real test environment.**

IV. TEST EQUIPMENT AND EXPERIMENT SCENE

The communication between RSU and OBU in the ETC system usually employs microwaves at 5.8 GHz and 915 MHz. As presented in Figure 14, to improve the adaptability of test equipment, we developed an ETC comprehensive test instrument based on a software-defined radio platform, which can not only measure different wireless communication devices with various working frequencies but also simulate the tag or reader of a radio frequency identification (RFID) system [32]. The test instrument system contains an NI PXI-1065, and an NI PXI-8108 embedded controller that can run the LabVIEW application program [22], [33], [34], [35]. When the radio frequency (RF) signal generator of NI PXIe-5644 sends a query command to the RSU, the RF signal receiver can capture and process the response from the OBU. The NI PXIe-5640R IF RIO FPGA can establish the communication between RSU and OBU. Furthermore, the parameters of the antennas in the test instrument are depicted in Table 6.

Given the security and implementation of the experiment, we chose a toll station that is not yet open to traffic, as shown in Figure 15. The OBU should be placed on the upper half of windshield, especially on the middle of top ledge (microwave skylight), which is in accordance with the suggestion of

TABLE 6. Antennas parameters.

Parameters	Value
Frequency (GHz)	5.79-5.84
Bandwidth (MHz)	125
Gain (dBi)	16
VSWR	<1.5
Impedance (Ω)	50
Polarization	RHCP
Vertical beam-width ($^\circ$)	40
Horizontal beam-width ($^\circ$)	30

producer of OBU. The RSU is placed in the top position of the ETC lane of the toll station. To get closer to our experiment; we utilized Volkswagen Jetta cars and Xu Gong heavy trucks as our test vehicles. We conducted multiple measurements on all ray paths, taking the average value to ensure the minimum error. The distance between OBU and RSU varies from 100 m to 0 m with a step 1 m and each model was measured five times. Finally, we obtained the propagation losses of four models. We do not consider the interference of side vehicles, and defaults that the front and rear vehicles are in the same straight line.

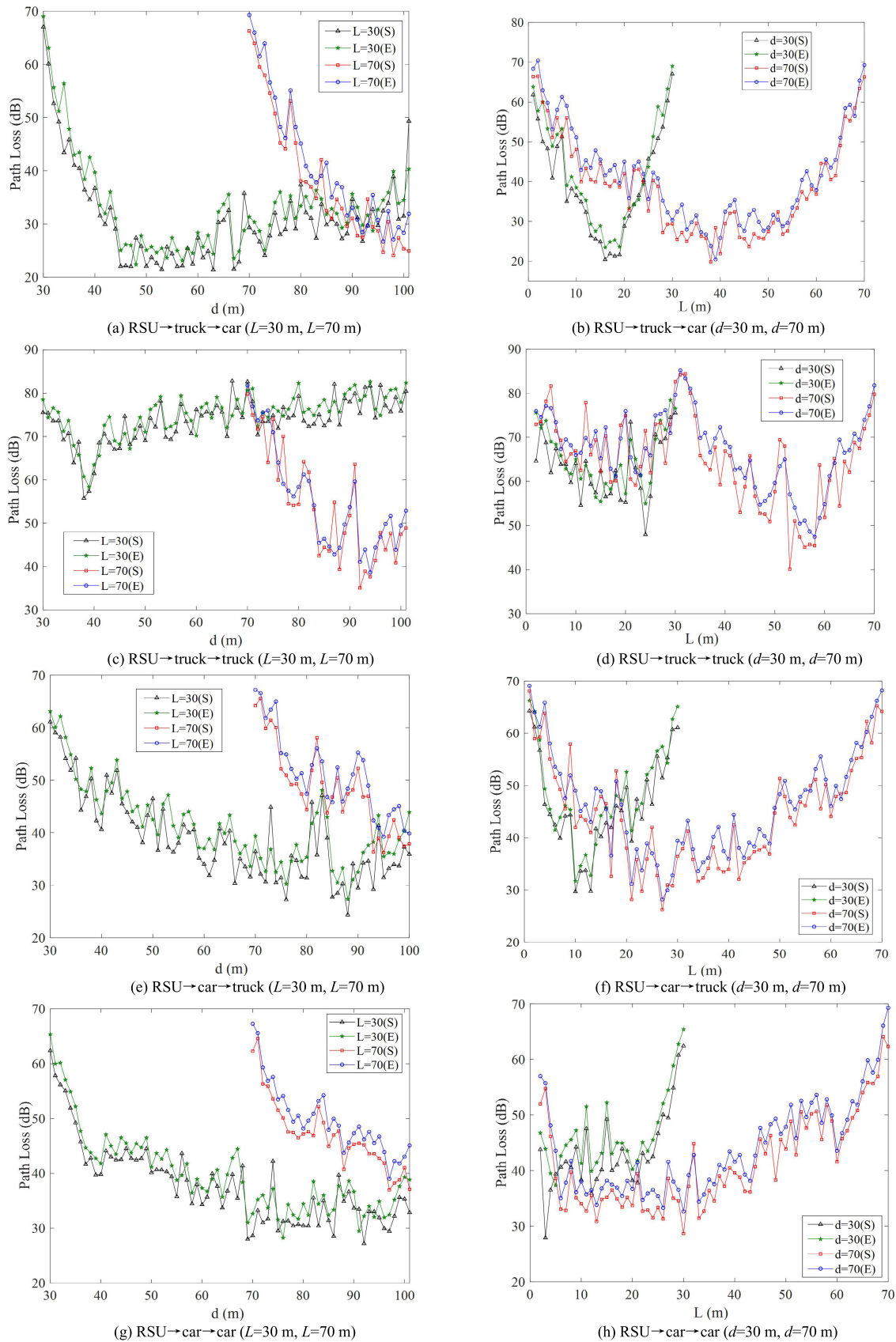


FIGURE 16. The propagation path loss of four propagation loss models.

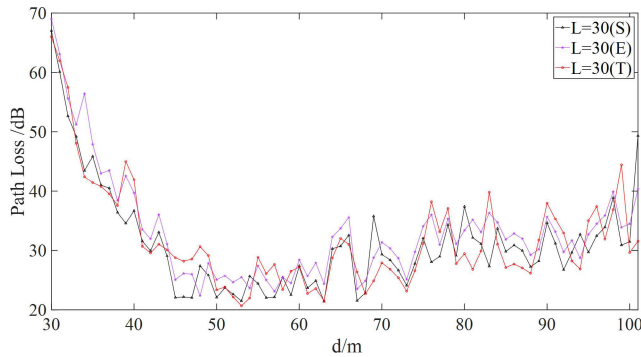


FIGURE 17. Experimental comparison.

TABLE 7. Comparison of errors between different algorithms.

Model	MAE	RMSE
This paper	2.8924	3.5689
Two-ray	3.3454	4.0003

Because of the massive workload for measuring all the distances of d and L in the actual road, we choose two values of d ($d = 30$ m, $d = 70$ m) and two values of L ($L = 30$ m, $L = 70$ m). We eventually get the propagation loss of the four models, as presented in Figure 16.

Figure 16 reveals that the trend of the experiment results is similar to the simulation results. S stands for simulation result. E stands for experimental results. T stands for Two-ray. The average error between simulation and measurement results is less than 5 dB, induced by the test equipment, the vehicle geometric features' irregularity, and the surrounding infrastructure's interference. In some cases, the error is greater than 10dB. The propagation loss is related to the distance and frequency f . The received signal is the vector sum of direct, reflected, and diffracted signals. Due to the high operating frequency and short wavelength of the radio wave, a measurement error or the displacement of a few centimeters of the RSU/OBU antennas may cause the response in (2) to be completely different.

In order to verify the feasibility of the model proposed in this paper, the model is compared with the actual measurement results and the two-ray model. As shown in Figure 17 and TABLE 7, compared with the two-ray model, the mean absolute error (MAE) and root mean square error (RMSE) of the model are smaller, therefore, the accuracy and performance of this algorithm are higher.

V. CONCLUSION

In this paper, we mainly explore the interference of the front vehicle in the ETC communication system. Considering the geometric characteristics of the vehicle, we divide the ETC application into four different scenarios. The results demonstrate that: (1) the geometric features of vehicles (the front vehicle and the object vehicle) have effects primarily on the reflected path and diffracted path; (2) the relative location among RSU, the front vehicle, and OBU is the critical factor

in determining the presence (LOS condition) or non-existence (NLOS condition) of the direct path; (3) when L increases, and d remains unchanged, or d rises, and L is constant, the propagation loss changes from high to low, and then to high. Therefore, based on the path loss results as a function of d and L in the four propagation loss models, we can obtain a lower path loss region for the ETC communication system.

The ETC system discussed in this paper is a single-lane mode in which the vehicle passes through the toll station at a low speed (less than 20 km/h). With the development of ITS, the Multi-Lane Free-Flow (MLFF) will gradually become mainstream, where the vehicle does not need to slow down to pass through the ETC. Accordingly, the influence of the vehicles in adjacent lanes and the Doppler effect caused by vehicle speed cannot be neglected. In future research, we will study the impact of adjacent lanes and the Doppler effect on ETC communication.

REFERENCES

- [1] M. Wazid, B. Bera, A. K. Das, S. P. Mohanty, and M. Jo, "Fortifying smart transportation security through public blockchain," *IEEE Internet Things J.*, vol. 9, no. 17, pp. 16532–16545, Sep. 2022.
- [2] Y. Dong, X. Cai, and G. Wen, "Circularly polarized antenna array with suppressed sidelobes for electronic toll collection," *IEEE Antennas Wireless Propag. Lett.*, vol. 21, no. 5, pp. 988–992, May 2022.
- [3] W. Huang, L. Ding, D. Meng, J.-N. Hwang, Y. Xu, and W. Zhang, "QoE-based resource allocation for heterogeneous multi-radio communication in software-defined vehicle networks," *IEEE Access*, vol. 6, pp. 3387–3399, 2018.
- [4] W. Viriyasitavat, M. Boban, H.-M. Tsai, and A. Vasilakos, "Vehicular communications: Survey and challenges of channel and propagation models," *IEEE Veh. Technol. Mag.*, vol. 10, no. 2, pp. 55–66, Jun. 2015.
- [5] D. Salós, A. Martineau, C. Macabiau, B. Bonhoure, and D. Kubrak, "Receiver autonomous integrity monitoring of GNSS signals for electronic toll collection," *IEEE Trans. Intell. Transp. Syst.*, vol. 15, no. 1, pp. 94–103, Feb. 2014.
- [6] V. Milanés, J. Villagra, J. Godoy, J. Simo, J. Perez, and E. Onieva, "An intelligent V2I-based traffic management system," *IEEE Trans. Intell. Transp. Syst.*, vol. 13, no. 1, pp. 49–58, Mar. 2012.
- [7] M. Zhang, R. Liu, Y. Zhang, W. Wang, H. Liu, and C. Lu, "A fully integrated RSSI and an ultra-low power SAR ADC for 5.8 GHz DSRC ETC transceiver," *AEU Int. J. Electron. Commun.*, vol. 86, pp. 154–163, Mar. 2018.
- [8] J. B. Kenney, "Dedicated short-range communications (DSRC) standards in the United States," *Proc. IEEE*, vol. 99, no. 7, pp. 1162–1182, Jul. 2011.
- [9] J.-C. Lin, C.-S. Lin, C.-N. Liang, and B.-C. Chen, "Wireless communication performance based on IEEE 802.11p R2V field trials," *IEEE Commun. Mag.*, vol. 50, no. 5, pp. 184–191, May 2012.
- [10] D. Jiang, V. Taliwal, A. Meier, W. Holfelder, and R. Herrtwich, "Design of 5.9 GHz DSRC-based vehicular safety communication," *IEEE Wireless Commun.*, vol. 13, no. 5, pp. 36–43, Oct. 2006.
- [11] C. F. Mecklenbrauker, A. F. Molisch, J. Karedal, F. Tufvesson, A. Paier, L. Bernado, T. Zemen, O. Klemp, and N. Czink, "Vehicular channel characterization and its implications for wireless system design and performance," *Proc. IEEE*, vol. 99, no. 7, pp. 1189–1212, Jul. 2011.
- [12] A. G. Zajic, "Impact of moving scatterers on vehicle-to-vehicle narrow-band channel characteristics," *IEEE Trans. Veh. Technol.*, vol. 63, no. 7, pp. 3094–3106, Sep. 2014.
- [13] D. Vlastaras, T. Abbas, M. Nilsson, R. Whiton, M. Olbäck, and F. Tufvesson, "Impact of a truck as an obstacle on vehicle-to-vehicle communications in rural and highway scenarios," in *Proc. IEEE 6th Int. Symp. Wireless Veh. Commun. (WiVeC)*, Sep. 2014, pp. 1–6.
- [14] S. A. Hosseini Tabatabaei, M. Fleury, N. N. Qadri, and M. Ghanbari, "Improving propagation modeling in urban environments for vehicular ad hoc networks," *IEEE Trans. Intell. Transp. Syst.*, vol. 12, no. 3, pp. 705–716, Sep. 2011.

- [15] T. Abbas, J. Karedal, F. Tufvesson, A. Paier, L. Bernado, and A. F. Molisch, "Directional analysis of Vehicle-to-Vehicle propagation channels," in *Proc. IEEE 73rd Veh. Technol. Conf. (VTC Spring)*, May 2011, pp. 1–5.
- [16] I. Sen and D. W. Matolak, "Vehicle-vehicle channel models for the 5-GHz band," *IEEE Trans. Intell. Transp. Syst.*, vol. 9, no. 2, pp. 235–245, Jun. 2008.
- [17] W. Zhang, "A wide-band propagation model based on UTD for cellular mobile radio communications," *IEEE Trans. Antennas Propag.*, vol. 45, no. 11, pp. 1669–1678, Nov. 1997.
- [18] R. He, A. F. Molisch, F. Tufvesson, Z. Zhong, B. Ai, and T. Zhang, "Vehicle-to-vehicle propagation models with large vehicle obstructions," *IEEE Trans. Intell. Transp. Syst.*, vol. 15, no. 5, pp. 2237–2248, Oct. 2014.
- [19] M. Boban, T. T. V. Vinhoza, M. Ferreira, J. Barros, and O. K. Tonguz, "Impact of vehicles as obstacles in vehicular ad hoc networks," *IEEE J. Sel. Areas Commun.*, vol. 29, no. 1, pp. 15–28, Jan. 2011.
- [20] R. Schmitz, A. Leiggenger, A. Festag, L. Eggert, and W. Effelsberg, "Analysis of path characteristics and transport protocol design in vehicular ad hoc networks," in *Proc. IEEE 63rd Veh. Technol. Conf.*, May 2006, pp. 528–532.
- [21] K. Guan, D. He, B. Ai, D. W. Matolak, Q. Wang, Z. Zhong, and T. Kürner, "5-GHz obstructed vehicle-to-vehicle channel characterization for Internet of intelligent vehicles," *IEEE Internet Things J.*, vol. 6, no. 1, pp. 100–110, Feb. 2019.
- [22] B. Gallagher, H. Akatsuka, and H. Suzuki, "Wireless communications for vehicle safety: Radio link performance and wireless connectivity methods," *IEEE Veh. Technol. Mag.*, vol. 1, no. 4, pp. 4–24, Dec. 2006.
- [23] B. Li, Q. Huan, L. Zuo, B. Yin, F. Guo, and Y. He, "Impact of vehicle head geometric features in the propagation loss of ETC system," *IEEE Intell. Transp. Syst. Mag.*, vol. 9, no. 3, pp. 88–99, Fall. 2017.
- [24] W.-Y. Shieh, C. J. Hsu, and T.-H. Wang, "A problem of infrared electronic-toll-collection systems: The irregularity of LED radiation pattern and emitter design," *IEEE Trans. Intell. Transp. Syst.*, vol. 12, no. 1, pp. 152–163, Mar. 2011.
- [25] M. G. Nilsson, C. Gustafson, T. Abbas, and F. Tufvesson, "A measurement-based multilink shadowing model for V2V network simulations of highway scenarios," *IEEE Trans. Veh. Technol.*, vol. 66, no. 10, pp. 8632–8643, Oct. 2017.
- [26] D. Yan, K. Guan, D. He, J. Kim, H. Chung, D. Tian, and Z. Zhong, "Blockage effects of road bridge on mmWave channels for intelligent autonomous vehicles," *IEEE Trans. Intell. Transp. Syst.*, early access, May 12, 2023, doi: [10.1109/TITS.2023.3271133](https://doi.org/10.1109/TITS.2023.3271133).
- [27] S. Loyka and A. Kouki, "Using two ray multipath model for microwave link budget analysis," *IEEE Antennas Propag. Mag.*, vol. 43, no. 5, pp. 31–36, Oct. 2001.
- [28] S. Grubisic, W. P. Carpes, C. B. Lima, and P. Kuo-Peng, "Ray-tracing propagation model using image theory with a new accurate approximation for transmitted rays through walls," *IEEE Trans. Magn.*, vol. 42, no. 4, pp. 835–838, Apr. 2006.
- [29] P. D. Holm, "A new heuristic UTD diffraction coefficient for nonperfectly conducting wedges," *IEEE Trans. Antennas Propag.*, vol. 48, no. 8, pp. 1211–1219, Aug. 2000.
- [30] P. H. Pathak, G. Carluccio, and M. Albani, "The uniform geometrical theory of diffraction and some of its applications," *IEEE Antennas Propag. Mag.*, vol. 55, no. 4, pp. 41–69, Aug. 2013.
- [31] C.-x. Wang, X. Cheng, and D. I. Laurenson, "Vehicle-to-vehicle channel modeling and measurements: Recent advances and future challenges," *IEEE Commun. Mag.*, vol. 47, no. 11, pp. 96–103, Nov. 2009.
- [32] L. Catarinucci, D. De Donno, R. Colella, F. Ricciato, and L. Tarricone, "A cost-effective SDR platform for performance characterization of RFID tags," *IEEE Trans. Instrum. Meas.*, vol. 61, no. 4, pp. 903–911, Apr. 2012.
- [33] R. Colella, L. Catarinucci, P. Coppola, and L. Tarricone, "Measurement platform for electromagnetic characterization and performance evaluation of UHF RFID tags," *IEEE Trans. Instrum. Meas.*, vol. 65, no. 4, pp. 905–914, Apr. 2016.
- [34] P. V. Nikitin and K. V. S. Rao, "LabVIEW-based UHF RFID tag test and measurement system," *IEEE Trans. Ind. Electron.*, vol. 56, no. 7, pp. 2374–2381, Jul. 2009.
- [35] J. D. Griffin and G. D. Durgin, "Complete link budgets for backscatter-radio and RFID systems," *IEEE Antennas Propag. Mag.*, vol. 51, no. 2, pp. 11–25, Apr. 2009.
- [36] D. Kandimalla, A. De, and S. Sanyal, "A novel UTD-type diffraction coefficient for a straight edge in a curved screen," *IEEE Trans. Antennas Propag.*, vol. 63, no. 3, pp. 1172–1177, Mar. 2015.
- [37] M. Albani, G. Carluccio, and P. H. Pathak, "A uniform geometrical theory of diffraction for vertices formed by truncated curved wedges," *IEEE Trans. Antennas Propag.*, vol. 63, no. 7, pp. 3136–3143, Apr. 2015.



XIAOYU LI was born in Hunan, China, in January 2000. He is currently pursuing the degree with The University of British Columbia, Vancouver, Canada, from 2019. His research interests mainly include wireless communication channel modeling, wireless sensing, and machine learning in wireless communications.



WENBO ZENG was born in Hunan, China, in August 1994. He received the bachelor's degree from Hunan University, Changsha, China, in 2016, and the Ph.D. degree in electrical engineering from the Hefei University of Technology, Hefei, China, in 2021. In 2022, he joined the School of Electronic Information and Electrical Engineering, Changsha University, Changsha. His research interests mainly include wireless communication channel modeling, wireless sensing, and machine learning in wireless communications.



HUAWEI LIANG received the Ph.D. degree in detection technology and automation from the University of Science and Technology of China, Hefei, China, in 2007. He is currently a Principal Investigator and the Deputy Director of the Institute of Intelligent Machines, Hefei Institutes of Physical Science, Chinese Academy of Science, Hefei. He has been engaged in the robotics, intelligent vehicle technology, detection technology and automation device, pattern recognition and intelligent systems, control theory, and control engineering.

...